ISSN: 2633-4828 Vol. 5 No.4, December, 2023

International Journal of Applied Engineering & Technology

ANALYZING THE ELECTRICAL RESISTIVITY OF RARE-EARTH (HO3+) SUBSTITUTED NANO-SIZED $COFE_2O_4$ DC

Aarti Lokhande* and Dr. Ritesh Yadav
Department of Physics, Dr. A.P.J. Abdul Kalam University, Indore (M.P.) – 452010
*artiram199.5@gmail.com

ABSTRACT
This study investigates the electrical resistivity properties of nano-sized CoFe2O4 (CFO) with rare-earth element Holmium (Ho3+) substitution. CFO is a well-known ferrite material with promising applications in various fields, including electronics and telecommunications, owing to its unique magnetic and electrical properties. In this research, we synthesized Ho3+-substituted CFO nanoparticles through a co-precipitation method, aiming to tailor and enhance the electrical characteristics of CFO for specific applications. The synthesis process was systematically characterized through X-ray diffraction (XRD), scanning electron microscopy (SEM), energy-dispersive X-ray spectroscopy (EDX), and Fourier-transform infrared spectroscopy (FTIR). The XRD analysis confirmed the formation of a single-phase spinel structure, and SEM images revealed well-dispersed nanoparticles. EDX and FTIR analyses confirmed the successful substitution of Ho3+ ions in the CFO lattice. The electrical resistivity of the synthesized Ho3+-substituted CFO was assessed using a four-point probe method, and the results were compared with pristine CFO. The investigation revealed that the Ho3+ substitution influenced the electrical properties of CFO significantly. The resistivity was found to be dependent on the concentration of Ho3+ ions, and an optimal substitution level was identified. This research sheds light on the potential use of Ho3+-substituted CFO in applications that require tailored electrical characteristics, such as inductor cores and microwave devices. The findings from this study offer valuable insights into the tunability of CFO's electrical properties through rare-earth element substitution, making it a promising candidate for a wide range of advanced electronic applications.

Keywords: Magnetic, Optimal, Electrical, Resistivity, Fourier-transform infrared spectroscopy

INTRODUCTION
Exchange interactions between spinel ferrites and rare earth (RE) transition metal (4f-3d) elements have been the subject of much theoretical and experimental study in recent decades. Larger ionic radii, unpaired 4f electrons, and magneto-crystalline anisotropy triggered by 4f-3d coupling as a result of exchange contact all play a role in this phenomenon. It has been reported in the literature that the addition of Ho3+ ions to CFO increases the saturation magnetization and coercivity of the compound. This improvement is likely the result of the greater magnetic moment of the Ho3+ ions and the increased exchange contact between them. Ho3+ doped CFO samples were also found to have a much higher dielectric constant and a very low loss factor at high frequencies. It has been shown in the literature that even when using optimal synthesis settings in the sol-gel reaction technique, a secondary HoFeO3 phase will emerge alongside the cubic spinel phase. HoFeO3 peaks with increasing Ho3+ substitution was identified in samples of holmium substituted cobalt ferrite prepared by Ghone et al. utilizing the chemical co-precipitation process. Saturation magnetization, coercivity, and retentivity were shown to decrease with increasing Holmium concentration in magnetic experiments taken at room temperature, suggesting the participation of mild A-B exchange interactions (CoHoxFe2–xO4 (x = 0.00, 0.05, 0.1, 0.15, 0.2)).

Our research is motivated by a desire to improve high-frequency electromagnetic and magneto-recording systems by increasing the dielectric constant of RE-doped CFO relative to pure CFO without compromising its insulating capabilities. Based on the above, we have studied the effects of replacing the Fe in CFO with Holmium (Ho3+) and examining its structural, electrical, dielectric, magnetic, and Mössbauer characteristics. In this regard, the glycine-nitrate synthesis technique is used to complete the current study. Materials with high purity, homogeneity,

and nano-scale structure may be produced with this process thanks to the self-combustion of metal nitrate and glycine.

EXPERIMENTAL PROCEDURE

The glycine nitrate auto-combustion approach yielded a sequence of CoFe2-xHoxO4 (CFHO) (where x = 0, 0.1, 0.3, 0.5, 0.7). Cobalt nitrate (Co(NO3)2.6H2O), holmium nitrate (Ho(NO3)3.5H2O), and ferric nitrate (Fe(NO3)2.9H2O) were combined to create CoFe2-xHoxO4. All chemicals used were of 99% purity and were bought from Sigma-Aldrich. Our previous works provide detailed illustrations of the experimental approach. The resulting powder was calcined at 600 degrees Celsius for three hours. Rigaku Ultima-IV X-Ray Diffractometer (XRD) (CuK radiation, k = 1.54 Å) X-ray analysis of CFHO powder samples. Nova NanoSEM-450 Field emission scanning electron microscopy (FESEM) and FEI MODEL-TECNAI TF 30 G2 Transmission electron microscopy (TEM) was used to examine the particle surfaces and determine their composition. The H20KI LCR meter (IM3570) was used to conduct electrical and dielectric tests from ambient temperature (30 ^{o}C) to 300 ^{o}C. Temperature at rest. The 7400 series vibrating sample magnetometer (VSM) from Lake Shore Cryotronics was used to analyze the magnetic readings. Powder samples were analyzed by a Mössbauer spectrometer at VECC, Kolkata, using a Co source.

3.3. RESULTS AND DISCUSSION

3.3.1. X-Ray Diffraction (XRD) Analysis

Figure 1 displays the XRD pattern obtained from CFHO nanoferrites. All of the peaks found were assigned miller indices in the range from 111 to 533, making them a spinel cubic in the Fd3m space group. Secondary peak (marked ◆ and un-indexed peak) and trace amounts of ortho-ferrite phase (HoFeO3) occur with increasing Ho3+ concentration (x ≥0.5). The greater ionic radius of the Ho3+ ions (0.901 Å) substituted for the smaller ionic radius of the Fe3+ (0.76 Å), leading to an increase in the lattice constant with increasing Ho concentration. Crystallite size (D) was determined using Debye Scherer's equation, shown as Equation (1), and tabulated below. 1:

$$D = \frac{K\lambda}{B\cos\theta} \quad (1)$$

where K, λ, β, θ are K = 0.9, the wavelength, the full width at half maximum (FWHM), and the Bragg angle, all of which are dimensionless.

After XRD patterns were refined, the following formula was used to get the experimental lattice parameter:

$$a_{exp} = d/\sqrt{(h^2 + k^2 + l^2)}$$

Miller indices (h, k, l) and inter-planar distance (d) are used.

The following connection, which connects the cation radius of the component elements at the various lattice sites to the lattice parameter, may be used to theoretically (ath) determine the lattice parameter:

$$a_{th} = \frac{8}{3\sqrt{3}}\left[(r_A + R_0) + \sqrt{3}(r_B + R_0)\right]\text{Å}$$

where R0 is the radius of the oxygen ion (1.32 Å).

The radius of the tetrahedral site, rA, is calculated as follows:

$$r_A = [f_c(Co^{2+}) \cdot r(Co^{2+}) + f_c(Fe^{3+}) \cdot r(Fe^{3+}) + f_c(Ho^{3+}) \cdot r(Ho^{3+})]\text{Å}$$

The octahedral site radius is denoted by rB.

$$r_B = \frac{1}{2}[f_c(Co^{2+}) \cdot r(Co^{2+}) + f_c(Fe^{3+}) \cdot r(Fe^{3+}) + f_c(Ho^{3+}) \cdot r(Ho^{3+})]\text{Å}$$

where f c denotes fractional concentrations, r denotes ionic radii, and r (Co2+) = 0:745 Å, (r Fe3+) = 0:645 Å, (r Ho3+) = 0:901 Å.

Tabulated in Table 1 are the theoretically determined values of rA, rB, and ath derived from the aforementioned equations, which show a consistent pattern with the experimental data. According to Vegard's law, the lattice expands and the lattice constant rises if the radius of the displacing ion is bigger than that of the displaced ion. In accordance with the Vegard rule, which suggests the integration of Ho3+ in the spinel structure, the lattice parameter grows linearly with increasing Ho3+ concentration, as shown by the structural parameter refinement provided by the Rietveld technique. As Ho concentration (H) increased, smaller crystals were obtained (D). The lattice constant is observed to grow with RE substitution compared to pure CFO. This is because RE ions, which are introduced at the spinel lattice's octahedral location, have bigger radii than Fe3+ ions. The percentage of Co2+, Fe3+, and RE3+ cations in a spinel is directly related to the lattice parameter value and the cation-anion distance for a certain location in the spinel structure. Therefore, the lattice parameter may grow as the amount of RE grows.

The presence of RE3+ ions near the grain borders, which impedes grain development and applies pressure on the grain, is responsible for the observed decrease in crystallite size. The Williamson-Hall equation for peak broadening (β), given by the relation (2), was used to get an approximation of the strain value (e):

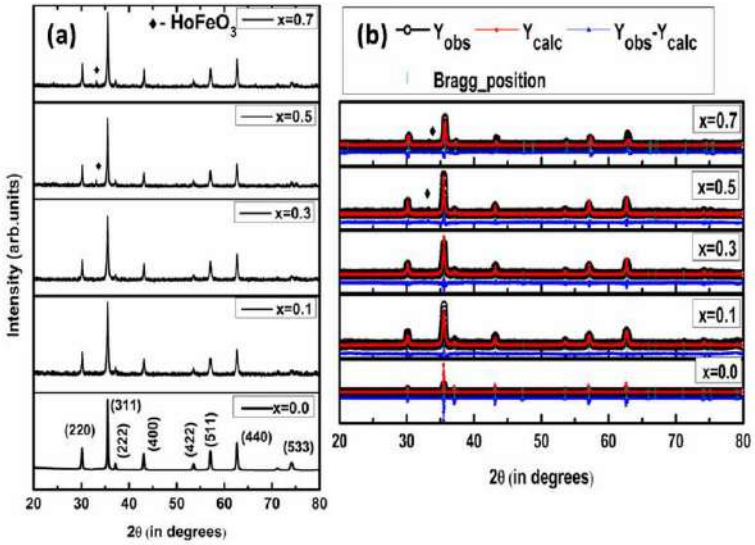

Figure 1. a) CoFe2-xHoxO4 (x = 0, 0.1, 0.3, 0.5, 0.7) X-ray diffraction patterns b) associated Rietveld refinement patterns

$$\beta \cos\theta = \frac{0.9\lambda}{D} + 4\varepsilon \sin\theta \quad (2)$$

where ε is the microstrain and 4 ε sinθ is the strain effect. The strain was calculated by observing the slope of a graph of 4sinθ. Using linear best fitting, the Williamson-Hall plots for CFHO are shown in Figure 2 for all observable peaks. The lattice strain value in Table 1 is derived from the linear slope of Williamson-Hall plots. Compressive strain, represented by negative strain values, is clearly visible in CFHO samples.

3.3.2. FTIR Analysis

Temperament normal Figure 2 shows the FT-IR spectra of CFHO for the following x values: 0, 0.1, 0.3, 0.5, and 0.7. As a result of the presence of two different symmetric sites, tetrahedral (583 cm^{-1}) and octahedral (411 cm^{-1}) peaks may be seen in FT-IR spectra of spinel ferrites. The appearance of these peaks is consistent with the production of spinel CFO and is reminiscent of metal-oxygen bonding; moreover, their frequencies are consistent with those described in the literature. Peaks at 2894 cm-1, 2850 cm-1, and 1636 cm-1 imply the existence of O-H bonds, C550 bonds, and O-C55O bonds, respectively, suggesting that hydroxyl and carboxyl functional groups are the most likely to be present. The O─H stretching is responsible for the absorption bands at 1636 cm^{-1}. Spectra showing a wide band between 2894 and 2850 cm^{-1} have been linked to C─H stretching. Differences in bond length between Fe3+ and O2 at tetrahedral A-sites and octahedral B-sites account for the bands' varying intensities.

Since Ho3+ and Fe3+ ions have the same propensity for occupying the octahedral sites, the replacement of Ho3+ does not result in a substantial difference in the tetrahedral stretching frequency. When examining the octahedral sites at 400 cm^{-1}, we see that when the Ho concentration rises, the peak values move up in wave number. The strain created by Ho doping in CFO causes the Fe3+ ions to migrate from tetrahedral positions to octahedral sites, expanding the radii of the ions in both structures.

Table 1: Nanoparticles of CoFe2-xHoxO4 ferrite (x = 0, 0.1, 0.3, 0.5, 0.7) crystallite size (D), lattice constant (a), and strain (e) values computed.

Sample composition	Site ionic radii		D (in nm)±0.1	a_{exp} (in Å)	a_{th} (in Å)	ε	Volume of unit cell $a=b=c$ (Å^3)
	A-site r_A (in Å)	B-site r_B (in Å)					
$CoFe_2O_4$	0.685	0.675	56.27	8.316±0.002	8.402	−0.0104±0.017	575.1
$CoFe_{1.90}Ho_{0.1}O_4$	0.696	0.682	35.40	8.346±0.001	8.433	−0.0617±0.021	581.3
$CoFe_{1.70}Ho_{0.3}O_4$	0.684	0.713	29.78	8.365±0.003	8.506	−0.0524±0.013	585.3
$CoFe_{1.50}Ho_{0.5}O_4$	0.613	0.774	22.91	8.379±0.002	8.559	−0.0513±0.011	588.2
$CoFe_{1.30}Ho_{0.7}O_4$	0.704	0.754	22.09	8.387±0.002	8.646	−0.0459±0.017	589.9

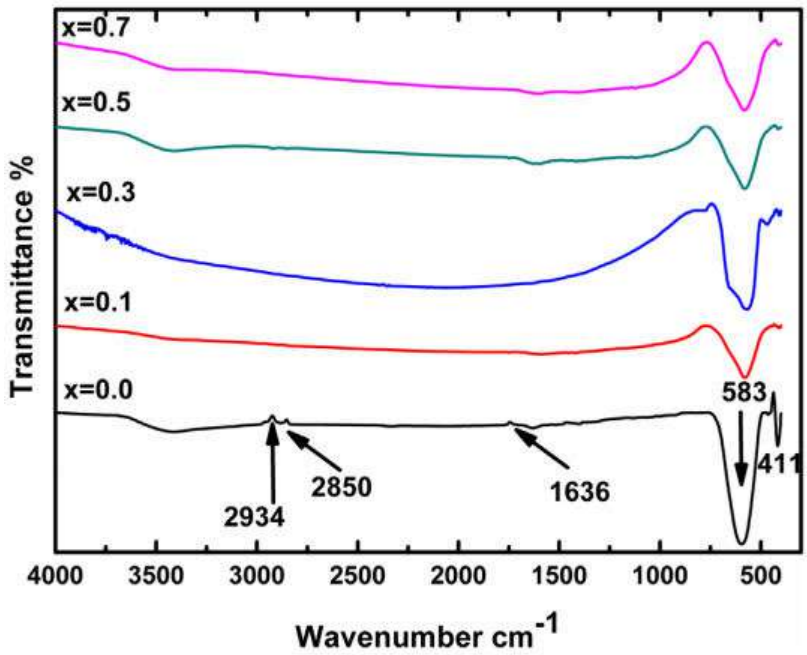

Figure 2: Nanoparticles of CoFe2-xHoxO4 ferrite were produced and their FT-IR spectra

Analysis using Transmission Electron Microscope (TEM) and Field Emission Scanning Electron Microscope (FESEM)

Figure 3 displays FESEM micrographs for more structural insight. Particles seem to be dispersed quite evenly throughout the FESEM micrographs. Consistent with the XRD findings, grain boundaries become more apparent with lower Ho contents, and grain size decreases with increasing dopant concentration. Due to the higher bond energy of Ho3+-O2- than Fe3+-O2-, more energy is needed to substitute Ho3+ ions in the CFO lattice to create Ho3+-O2-. Ho3+ replaced CFO samples have a harder time crystallizing and growing grains because they need more energy. In addition, the orthoferrite phase of HoFeO3 that forms at grain borders acts as pinning sites, preventing the grain from expanding and leading to the production of smaller grains.

Figure 4a(2)-e(2) displays TEM micrographs of CFHO nanoferrites, which may be used to further determine the particle size and shape of the produced nanoparticles. All the samples have a round, uniform shape and are distributed evenly. It seems that the majority of the nanoparticles are round and thin, however some are longer. This is because the micrographs show the FCC structure of the Ho3+ replaced CFO. Although magnetic nanoparticles interact with one another and are attracted to one another, the TEM micrographs reveal evidence of agglomeration where particles are piled on top of each other.

The average particle sizes were calculated from the measured particle diameters and are shown in Figure 4a(1)-e(1). The XRD measurements and the average size derived from the size distribution match well with a Gaussian distribution. The histograms confirm that the RE3+ substitution significantly reduces the particle size of CFO, which is consistent with the XRD findings. In addition, HRTEM images were used to study the synthesized materials for clues as to their shape and phase structure. Figure 4a(3)-e(3) displays typical HRTEM images of CFHO nanoparticles, demonstrating the great crystallinity of all samples by means of clearly visible lattice fringes.

According to the (311) crystalline planes of spinel ferrites, the crystal lattice spacing is calculated to be 0.225 ±0.002 nm, 0.241 ± 0.009 nm, 0.243 ± 0.002 nm, 0.251 ± 0.006 nm, 0.252±0.005 nm for CoFe2O4, CoFe1.9Ho0.1O4, CoFe1.7Ho0.3O4, CoFe1.5Ho0.5O4, and CoFe1.3 Ho0.7O4, respectively. Ho3+ substituted CFO nanoferrites are nanocrystalline and monodisperse, as seen by their uniformly parallel lattice fringes. Figure

4a(4)-e(4) displays EDS results showing that Fe, Co, O, and Ho are present in the samples. The incorporation of Ho3+ ions into the CFO is shown by these findings.

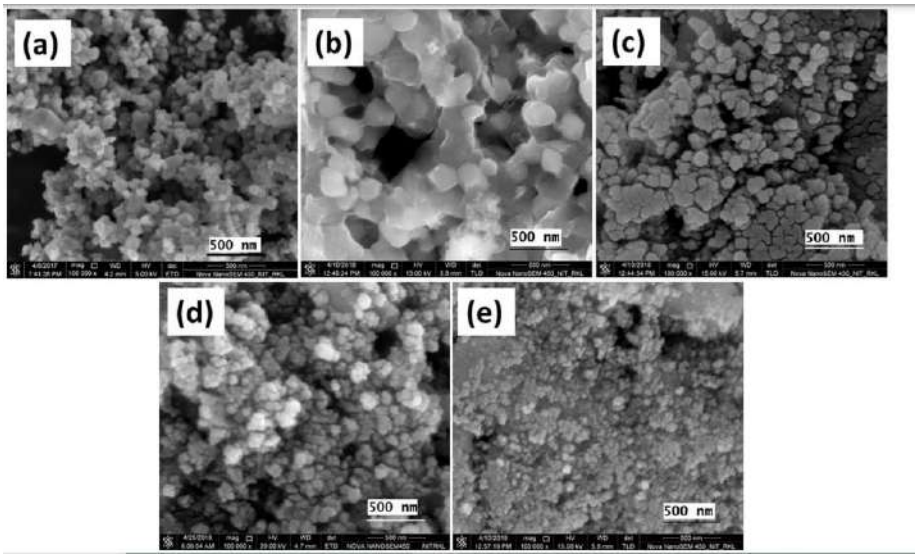

Figure 3: Nanoparticles of ferrite (a), CoFe2O4, (b) CoFe1.9Ho0.1O4, (c) CoFe1.7Ho0.3O4, (d) CoFe1.5Ho0.5O4, (e) CoFe1.3 Ho0.7O4 FESEM micrographs.

ELECTRICAL PROPERTIES

Impedance spectroscopy was used to get understanding into how the Ho substitution altered the electronic characteristics of CFO. The typical Nyquist plot of impedance for CFHO nanoferrites in the frequency domain of 100 Hz to 1 MHz is shown in Figure 5 over a range of temperatures from ambient temperature (30 ^{o}C) to 300 ^{o}C. There is always only one semicircle in Nyquist plots, and their centers never line up with the actual axis. The presence of the grain interior (bulk) property of the sample is indicated by the creation of a single semi-circular arc. CFHO nanoferrites are consistent with the Cole-Cole formalism, as seen by the decentralization of the semi-circular arcs. What this means is that there is just one mechanism at work in the electrical conduction.

The graphs suggest that the synthesized materials exhibit a typical semiconducting characteristic, negative temperature coefficient of resistance (NTCR), as seen by a decrease in bulk resistance with increasing temperature. This is because the conduction mechanism is improved due to a higher concentration of space charge carriers. This correlates with the observed change in microstructure, where grain size is shown to decrease along with rising Ho3+ concentration. Moreover, the thermal resistance of the CFHO nanoferrites may be reproduced by plotting Z'' = (Z') + at certain temperatures. As a result, conductivity increases as temperature rises. In general, the Nyquist representations are interpreted in order to establish a connection between the distinctive behaviors and the electrical equivalent circuit model. Figure 5's inset, a Nyquist plot of modulus as a function of frequency, provides more context for the conduction process and grain boundary impact.

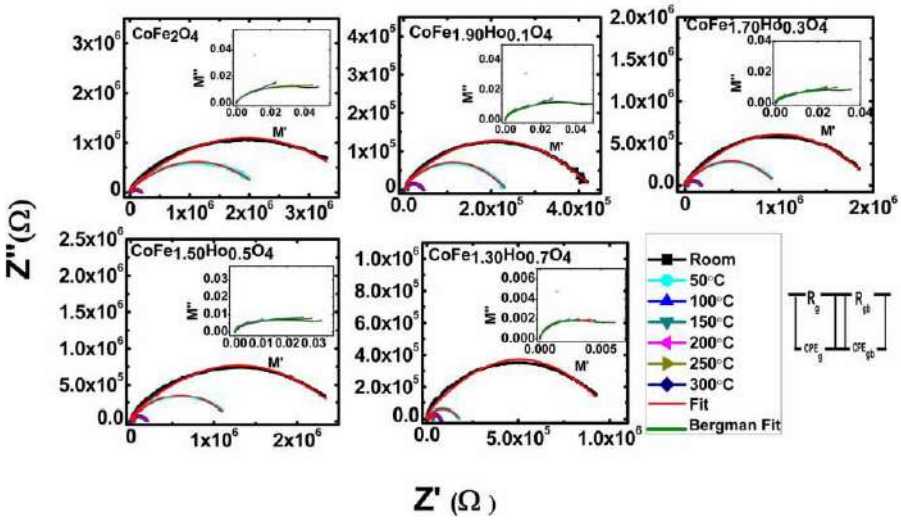

Figure 5: Nyquist plot of the equivalent circuit used to match the impedance curve of CoFe2-xHoxO4 ferrite nanoparticles at different chosen temperatures (x = 0, 0.1, 0.3, 0.5, 0.7). Modulus fitting Cole-Cole graphs at the same temperatures

A single semicircular arc appears in the graphs for all the chosen temperatures, representing the grain internal contribution. The semicircles, however, are poorly defined, and the maxima only appear at very low frequencies. According to the electric modulus, the Ho3+ replaced CFO samples do not experience the relaxation phenomena and, thus, suffer less loss as a result. The material's weak conductivity and low dielectric loss make CFHO well-suited for electromagnetic absorption applications; this low loss may be attributable to the occurrence of the relaxation peaks in the low frequency region. A plot of the real component of the impedance (Z') vs frequency over a range of operating temperatures is shown in Figure 6. It can be seen from the figures that Z' is greatest at low frequencies and diminishes with increasing creasein frequency. A decrease in Z' coincides with rising temperatures, indicating an improvement in the ac conductivity. Most of the overlap between Z' versus frequency charts occurs at very high frequencies. Z' is said to be merging because, as temperature rises, space charges are released and the material's barrier characteristics are lowered, resulting in increased ac conductivity.

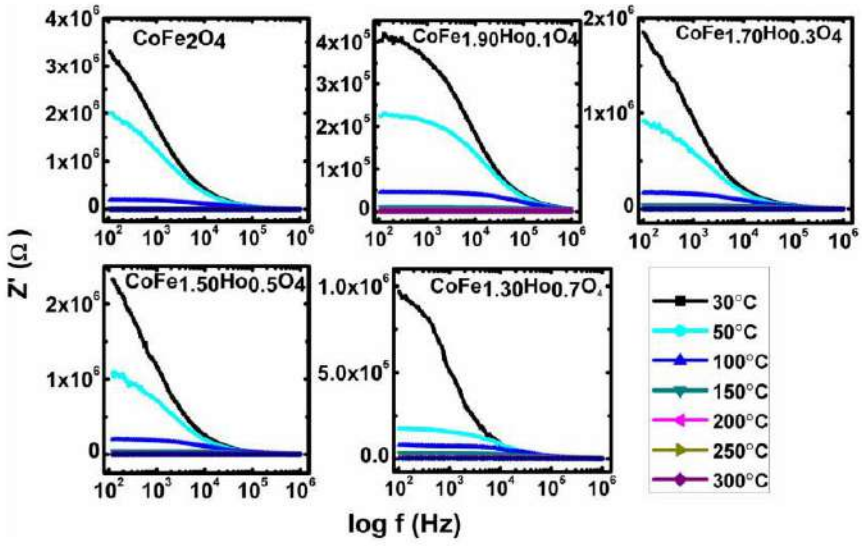

Figure 6: CoFe2-xHoxO4 ferrite nanoparticles (x = 0, 0.1, 0.3, 0.5, 0.7) exhibit temperature- and frequency-dependent changes in the real component of the impedance (Z')

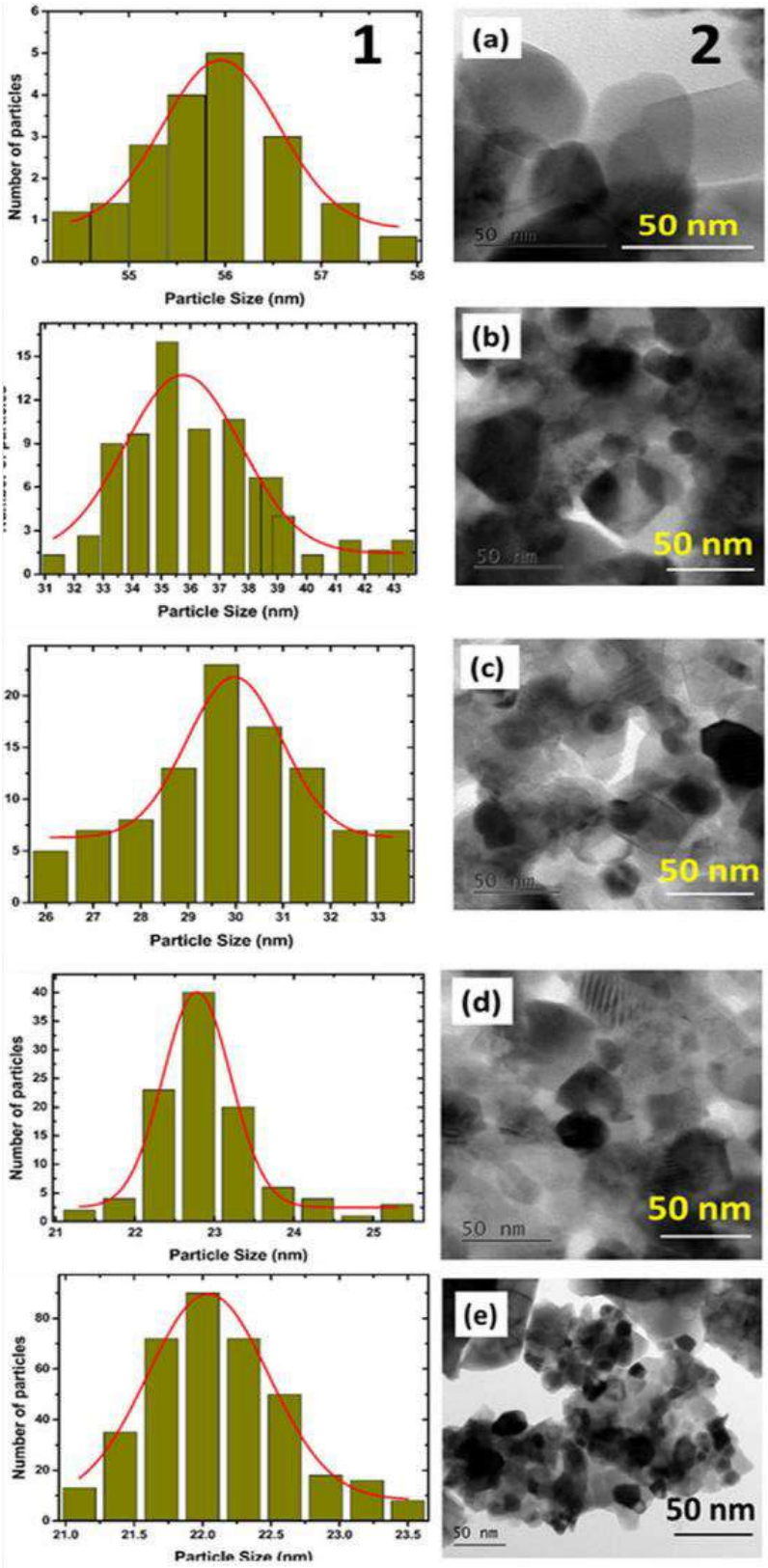
1
Number of particles
Particle Size (nm)
(a)
2
50 nm
(b)
50 nm
(c)
50 nm
(d)
50 nm
(e)
50 nm

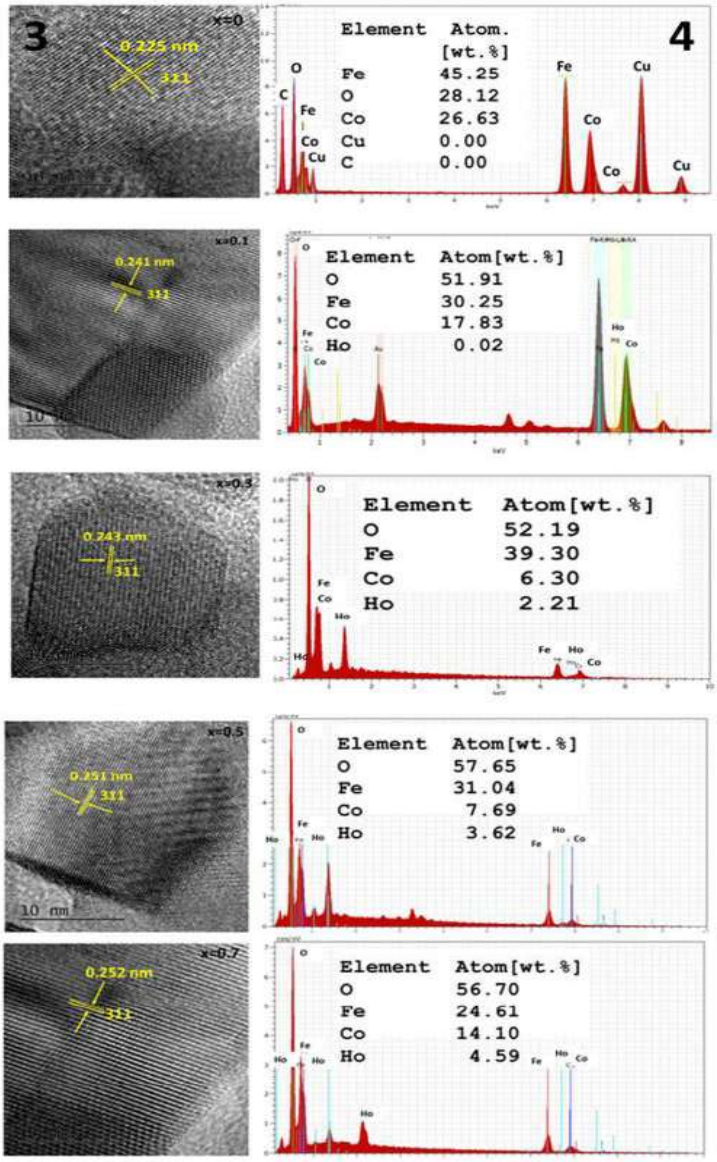

Figure 4: (1a–e) TEM micrographs (2a-e), high-resolution TEM (HRTEM) lattice pictures (3a-e), and the elemental analysis by EDX spectrum (4a-e) for CoFe2-xHoxO4 ferrite nanoparticles (where x = 0, 0.1, 0.3, 0.5, 0.7) are shown

CONCLUSION

In conclusion, the analysis of the electrical resistivity of rare-earth (Ho3+) substituted nano-sized CoFe2O4 (CFO) has provided valuable insights into the tunability of CFO's electrical properties and its potential for various electronic applications. This study synthesized Ho3+-substituted CFO nanoparticles and systematically characterized their structural and compositional properties. X-ray diffraction (XRD) analysis confirmed the formation of a single-phase spinel structure in the synthesized Ho3+-substituted CFO, while scanning electron microscopy (SEM) images revealed well-dispersed nanoparticles. Energy-dispersive X-ray spectroscopy (EDX) and Fourier-transform infrared spectroscopy (FTIR) analyses verified the successful substitution of Ho3+ ions within the CFO lattice. this research has contributed to our understanding of how rare-earth (Ho3+) substitution can be employed to enhance the electrical resistivity of nano-sized CoFe2O4, making it a versatile material for

electronic applications. The ability to tailor CFO's electrical properties to meet specific requirements in the electronics industry holds great promise for the development of high-performance components and devices. Further research in this direction could lead to even more specialized applications of this innovative material.

REFERENCES

1. R. C. Kambale, K. M. Song, C. J. Won, K. D. Lee, N. Hur, J. Cryst. Growth 2012, 340, 171.
2. G. Engdahl, Handbook of Giant Magnetostrictive Materials. Academic, San Diego 2000.
3. Y. Cedeño-Mattei, O. Perales-Perez, M. S. Tomar, F. Roman, P. M. Voyles, W. G. Stratton, J. Appl. Phys. 2008, 103, 07E512.
4. W. H. Von Aulock, C. E. Fay, Linear Ferrite Devices for Microwave Applications. Academic Press, New York 1968.
5. K. Raj, R.Moskowitz, R. Casciari, J. Magn.Magn. Mater. 1995, 149, 174.
6. R. Nongjai, S. Khan, K. Asokan, H. Ahmed, I. Khan, J. Appl. Phys. 2012, 112, 084321.
7. B. Zhou, Y.-W. Zhang, Y.-J. Yu, C.-S. Liao, C.-H. Yan, L.-Y. Chen, S.- Y. Wang, Phys. Rev. B 2003, 68, 024426.
8. B. H. Liu, J. Ding, Z. L. Dong, C. B. Boothroyd, J. H. Yin, J. B. Yi, Phys. Rev. B 2006, 74, 184427.
9. R. M. Bozorth, E. F. Tilden, A. J. Williums, Phys. Rev. 1955, 99, 1788.
10. D. S. Mathew, R. S. Juang, Chem. Eng. J. 2007, 129, 51.
11. P. P. Naik, Study of Structural, Magnetic and Electrical Properties of as Prepared and Gamma Iradiated Rare-Earth Doped Nanoparticle Ferrite Material, Doctoral dissertation, Goa University, 2017.
12. I. H. Gul, A. Maqsood, J. Alloys. Compd. 2008, 465, 227.
13. P. Kumar, S. K. Sharma, M. Knobel, M. Singh, J. Alloys Compd. 2010, 508, 115.
14. L. Kumar, P. Kumar, S. K. Srivastava, M. Kar, J. Supercond. Nov. Magn. 2014, 27, 1677.
15. L. Kumar, M. Kar, IEEE Trans. Magn. 2011, 47, 3645.
16. R. N. Pandaa,J. C. Shih, T. S. Chin, J.Magn. Magn.Mater. 2003, 257, 79.
17. M. H. Mahmoud, A. A. Sattar, J. Magn. Magn. Mater. 2004, 277, 101.
18. R. N. Bhowmik, R. Ranganathan, J. Alloys Compd. 2001, 326, 128.
19. J. Jensen, A. Mackintosh, Rare Earth Magnetism—Structures and Excitations, Clarendon, Oxford 1991.
20. M. H. Mahmouda, A. A. Sattar, J. Magn. Magn. Mater. 2004, 277, 101.
21. S. Urcia-Romero, O. Perales-Perez, G. Gutie´ rrez,´ J. Appl. Phys 2010, 107, 09A508.
22. K. K. Bharathi, G. Markandeyulu, C. V. Ramana, J. Phys. Chem. C 2010, 115, 554.
23. S. Supriya, S. Kumar, M. Kar, J. Appl. Phys. 2016, 120, 215106.
24. R. Kumar, M. Kar, Ceram. Int. 2016, 42, 6640.
25. S. Amiri, H. Shokrollahi, J. Magn. Magn. Mater. 2013, 345, 18.